Proceedings of the 2018 ASME International Conference and Exposition on Noise Control Engineering
NCAD2018
August 26-29, 2018, Chicago, IL, USA

NCAD2018-6134

AN ANALYTICAL AND NUMERICAL INVESTIGATION OF MODULATION SIDEBANDS OF A PLANETARY GEAR UNDER FLUCTUATED EXTERNAL TORQUE

Yunbo Yuan
College of Power and Energy Engineering
Harbin Engineering University
Harbin, China
yuanyunbo163@163.com

Wei Liu
College of Power and Energy Engineering
Harbin Engineering University
Harbin, China
liuwei@hrbeu.edu.cn

Yahui Chen
College of Power and Energy Engineering
Harbin Engineering University
Harbin, China
cyh163@ hrbeu.edu.cn

Donghua Wang*
College of Power and Energy Engineering
Harbin Engineering University
Harbin, China
hitwdh@163.com

ABSTRACT

Certain operating conditions such as fluctuation of the external torque to planetary gear sets can cause additional sidebands. In this paper, a mathematical model is proposed to investigate the modulation mechanisms due to a fluctuated external torque (FET), and the combined influence of such an external torque and manufacturing errors (ME) on modulation sidebands. Gear mesh interface excitations, namely gear static transmission error excitations and time-varying gear mesh stiffness, are defined in Fourier series forms. Amplitude and frequency modulations are demonstrated separately. The predicted dynamic gear mesh force spectra and radial acceleration spectra at a fixed position on ring gear are both shown to exhibit well-defined modulation sidebands. Comparing with sidebands caused by ME, more complex sidebands appear when taking both FET and ME into account. An obvious intermodulation is found around the fundamental gear mesh frequency between the FET and ME in the form of frequency modulations, however, no intermodulation in the form of amplitude modulations. Additionally, the results indicate that some of the sidebands are cancelled out in radial acceleration spectra mainly due to the effect of planet mesh phasing, especially when only amplitude modulations are present.

INTRODUCTION

Planetary gear transmission is commonly used in many fields such as automotive, aerospace and industrial applications. Compared with parallel-axes gear sets, planetary gear sets have many unique dynamic characteristics. Modulation sidebands, one of these unique dynamic characteristics, exits in most measured vibration and noise data of planetary gear sets. Three different forms of modulations, which include amplitude modulations (AM), frequency modulations (FM) and phase modulations (PM), were reported to occur frequently in mechanical systems [1, 2].

For AM of planetary gear sets, McFadden and Smith [3] proposed a model to explain for the asymmetric sidebands measured from accelerometers mounted to the housing of several planetary gear sets. Inalpolat and Kahraman [4] provided an analytical framework for predicting AM due to rotation of the carrier, they classified planetary gear sets based on their sideband behavior in five groups, and rules were established for sidebands for each category. AM effects of sidebands associated with rotation of the carrier were also investigated by McFadden [5] and McNames [6].

As for FM and PM, Mark and Hines [7] predicted the influence of planet-to-planet variability in planet/ring-gear loading due to a crack on the carrier posts on the sideband distributions. Inalpolat and Kahraman [8] established a nonlinear time-varying dynamic model to predict modulation sidebands, including FM due to a class of gear manufacturing errors (ME) and AM due to rotation of the carrier. They also

demonstrated the capability of such a model by measured planetary acceleration spectra.

The sidebands of planetary gear set were thought to be mostly caused by the carrier rotation [4-6], ME [8,9] and the unequal planet load sharing [7]. In recent studies, certain operating conditions such as fluctuation of the input torque to planetary gear sets were stated to cause additional sidebands [10,11]. To the authors' knowledge, however, any analytical formulation of modulations due to fluctuated speed or torque has not been available so far.

Accordingly, this study mainly aims at developing an analytical model to investigate the sidebands mechanisms of a two-stage planetary gear set due to the fluctuated external torque (FET) and the combined influence on modulations between the FET and ME. In order to gain a more in-depth investigation, amplitude and frequency modulations will be demonstrated separately.

DYNAMIC MODEL OF TWO-STAGE PLANETARY GEAR

A two-stage planetary gear set shown in Fig. 1 is considered in this paper. It is connected in series by two simple, single-stage planetary gears with standstill ring gears. The interactions between gear pairs are modeled by (i) periodically time-varying gear mesh stiffness, (ii) constant gear mesh damping, and (iii) periodic gear transmission error excitation. Bearings and interactions between two stages are modeled by linear springs.

A 2D discrete planar lumped-parameter dynamic model is considered here. For the sake of convenience, the model in this paper is based on an earlier model proposed by Lin and Parker [12], which was developed to investigate the natural frequencies and vibration modes of simple, single-stage planetary gear sets. However, some coupling models have been proposed to investigate the coupling vibration characteristics of multistage planetary gearbox [13,14]. Differing from the definition in Ref. [12], the rotational coordinates are defined to be θ_j, $(j = s, c, r, 1, 2, \cdots, n)$ rather than $u_j = r_j\theta_j$, for the convenience of the following study.

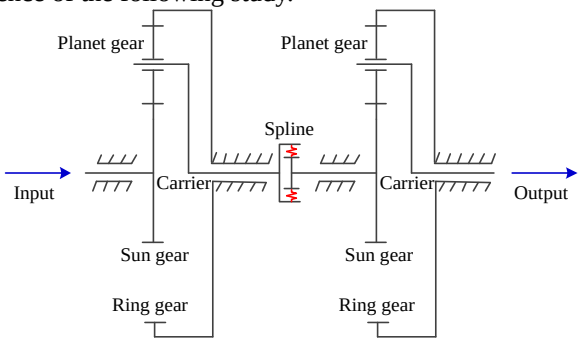

Fig. 1. Schematic of two-stage planetary gear set with standstill ring gears

As for the coupling effects between these two adjacent stages, they are described by a coupling stiffness matrix. To obtain such a matrix, two types of coordinate systems illustrated in Fig. 2 are created: (i) the absolute coordinate system OXY, (ii) the dynamic coordinate systems $Ox^{\mathrm{I}}y^{\mathrm{I}}$ rotating with the first-stage carrier and $Ox^{\mathrm{II}}y^{\mathrm{II}}$ rotating with the second-stage carrier. The relationships among these three coordinate systems are shown in Fig. 2. Defining the instantaneous angle between x^{I} and x^{II} as

$$\Phi^{\mathrm{I-II}} = \mathrm{mod}\left(\frac{\Omega_c^{\mathrm{I}}t - \Omega_c^{\mathrm{II}}t}{2\pi}\right) \tag{1}$$

where Ω_c^{I}, Ω_c^{II} are constant angular speeds of the first-stage carrier and the second-stage carrier, respectively.

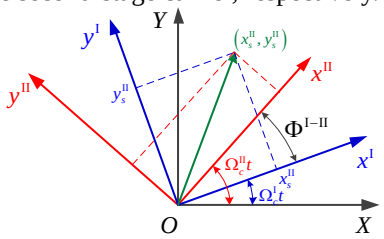

Fig. 2. Schematic of coordinate systems

According to the time-varying coordinate transformation between the carrier of first-stage and the sun of second-stage, equations of motion of these two components can be derived. With such equations available, one can get the coupling stiffness matrix as

$$\mathbf{K}_{\mathrm{I}}^{\mathrm{II}} = \begin{bmatrix} k_x & 0 & 0 \\ 0 & k_y & 0 \\ 0 & 0 & k_\theta (r_c^{\mathrm{I}})^2 \\ -k_x\cos\Phi^{\mathrm{I-II}} & k_x\sin\Phi^{\mathrm{I-II}} & 0 \\ -k_y\sin\Phi^{\mathrm{I-II}} & -k_y\cos\Phi^{\mathrm{I-II}} & 0 \\ 0 & 0 & -k_\theta r_c^{\mathrm{I}} r_s^{\mathrm{II}} \end{bmatrix}$$
$$\begin{bmatrix} -k_x\cos\Phi^{\mathrm{I-II}} & -k_x\sin\Phi^{\mathrm{I-II}} & 0 \\ k_y\sin\Phi^{\mathrm{I-II}} & -k_y\cos\Phi^{\mathrm{I-II}} & 0 \\ 0 & 0 & -k_\theta r_c^{\mathrm{I}} r_s^{\mathrm{II}} \\ k_x & 0 & 0 \\ 0 & k_y & 0 \\ 0 & 0 & k_\theta (r_s^{\mathrm{II}})^2 \end{bmatrix} \tag{2}$$

where k_x, k_y are the radial coupling stiffness, and k_θ is the torsional coupling stiffness. In this paper, the radial coupling stiffness is assumed to be equal ($k_x = k_y$).

Defining the displacement vector of the two-stage planetary gear set illustrated in Fig. 1 as

$$\mathbf{q} = \left\{ \begin{matrix} x_s^{\mathrm{I}}, y_s^{\mathrm{I}}, \theta_s^{\mathrm{I}}, x_r^{\mathrm{I}}, y_r^{\mathrm{I}}, \theta_r^{\mathrm{I}}, \xi_1^{\mathrm{I}}, \eta_1^{\mathrm{I}}, \theta_1^{\mathrm{I}}, \cdots, \xi_{N_{\mathrm{I}}}^{\mathrm{I}}, \eta_{N_{\mathrm{I}}}^{\mathrm{I}}, \theta_{N_{\mathrm{I}}}^{\mathrm{I}}, \\ x_c^{\mathrm{I}}, y_c^{\mathrm{I}}, \theta_c^{\mathrm{I}}, x_s^{\mathrm{II}}, y_s^{\mathrm{II}}, \theta_s^{\mathrm{II}}, x_r^{\mathrm{II}}, y_r^{\mathrm{II}}, \theta_r^{\mathrm{II}}, \xi_1^{\mathrm{II}}, \eta_1^{\mathrm{II}}, \theta_1^{\mathrm{II}}, \cdots, \\ \xi_{N_{\mathrm{II}}}^{\mathrm{II}}, \eta_{N_{\mathrm{II}}}^{\mathrm{II}}, \theta_{N_{\mathrm{II}}}^{\mathrm{II}}, x_c^{\mathrm{II}}, y_c^{\mathrm{II}}, \theta_c^{\mathrm{II}} \end{matrix} \right\}^T \tag{3}$$

Correspondingly, the governing equations for such a two-stage planetary gear set in matrix form are determined as Eq. (4a). However, one should notice that the coupling stiffness matrix $\mathbf{K}_{\mathrm{I}}^{\mathrm{II}}$ should be added to the overall stiffness matrix $\left[\mathbf{K}_b+\mathbf{K}_m(t)-\mathbf{\Omega}_c^2\mathbf{K}_\Omega\right]$ according to its local nodes.

$$\begin{aligned}&\mathbf{M}\{\ddot{\mathbf{q}}\}+\left[\mathbf{C}_b+\mathbf{C}_m+\mathbf{\Omega}_c\mathbf{G}\right]\{\dot{\mathbf{q}}\}\\&\quad+\left[\mathbf{K}_b+\mathbf{K}_m(t)-\mathbf{\Omega}_c^2\mathbf{K}_\Omega\right]\{\mathbf{q}\}=\mathbf{F}(t)+\mathbf{T}(t)\end{aligned}\tag{4a}$$

$$\mathbf{\Omega}_c=diag\left\{\left[\Omega_c^{\mathrm{I}}\right]_{(9+3N_{\mathrm{I}})\times(9+3N_{\mathrm{I}})},\ \left[\Omega_c^{\mathrm{II}}\right]_{(9+3N_{\mathrm{II}})\times(9+3N_{\mathrm{II}})}\right\}\tag{4b}$$

where $\mathbf{M}$, $\mathbf{G}$, $\mathbf{K}_\Omega$ are the mass, gyroscopic, and centrifugal stiffness matrices. $\mathbf{K}_b$, $\mathbf{C}_b$ are the elastic bearing stiffness and damping matrices. $\mathbf{K}_m(t)$, $\mathbf{C}_m$ are the time-varying gear mesh stiffness matrix and the constant gear mesh damping matrix. $\mathbf{F}(t)$ represents the dynamic gear mesh force vector, and $\mathbf{T}(t)$ denotes the vector of applied external forces and torques.

FORMULATION OF MODULATIONS OF THE EXCITATIONS

Transmission error excitations and mesh stiffness functions

A major excitation source in planetary gear sets comes from time-varying contact conditions at the gear tooth mesh interface as the gears engage kinematically. Gear static transmission error excitations, one of the major excitations of the gear tooth mesh interface, are defined in Fourier series form as [15]

$$e_{spn}(t)=\sum_{\ell=1}^{L}e_{sp}^{\ell}\sin\left[\ell\left(2\pi f_m t+Z_s\psi_n\right)+\phi_{sp}^{\ell}\right]\tag{5a}$$

$$e_{rpn}(t)=\sum_{\ell=1}^{L}e_{rp}^{\ell}\sin\left[\ell\left(2\pi f_m t+Z_r\psi_n+\gamma_{sr}\right)+\phi_{rp}^{\ell}\right]\tag{5b}$$

where all the parameters could be found in Ref. [15].

Periodically time-varying gear mesh stiffness functions, another of the major excitations of the gear tooth mesh interface, are defined in a similar form as [8]

$$k_{spn}(t)=\bar{k}_{sp}\left\{1+\sum_{\ell=1}^{L}k_{sp}^{\ell}\sin\left[\ell\left(2\pi f_m t+Z_s\psi_n+\Gamma\right)+\phi_{sp}^{\ell}\right]\right\}\tag{6a}$$

$$\begin{aligned}k_{rpn}(t)=\bar{k}_{rp}&\left\{1+\sum_{\ell=1}^{L}k_{rp}^{\ell}\right.\\&\left.\times\sin\left[\ell\left(2\pi f_m t+Z_r\psi_n+\Gamma+\gamma_{sr}\right)+\phi_{rp}^{\ell}\right]\right\}\end{aligned}\tag{6b}$$

The details for the parameters in Eq. (6) are given in Ref. [8].

Thus the mesh-frequency gear mesh forces can be defined as Eq. (7), without considering the shaft-frequency excitations contributed by manufacturing errors. Such errors include pitch-line run-out errors, gear eccentricities, tooth spacing and indexing errors.

$$F_{jpn}(t)=k_{jpn}(t)e_{jpn}(t)+c_{jpn}\dot{e}_{jpn}(t),\quad(j=s,r)\tag{7}$$

where c_{jpn} is the constant gear mesh damping and can be determined by the formula in Ref. [17]. For simplicity, in this paper, the gear mesh damping force component $c_{jpn}\dot{e}_{jpn}(t)$ is ignored.

Formulation of modulations due to the fluctuated external torque coupling with manufacturing errors

There are sharp interactions between the dynamic response to the distributed load as well as the load distribution. Some instances of such interactions are the tooth load distribution influencing the deflection of the carrier (and vice versa) [18,19]. As a result, the unequal planet load sharing under FET would cause additional sidebands, and such a phenomenon were reported in Ref. [10].

Only harmonic form FET is considered here, which is given as Eq. (8). However, one should realize that it may not be the case in some conditions.

$$T_{vet}(t)=\bar{T}_{vet}\left\{1+\sum_{\ell=1}^{L}\tau_{vet}^{\ell}\sin\left(2\pi f_{vet}^{\ell}t+\phi_{vet}^{\ell}\right)\right\}\tag{8}$$

where $\bar{T}_{vet}$ is the mean value of the FET, τ_{vet}^{ℓ} is the dimensionless amplitude at frequency f_{vet}^{ℓ}, and ϕ_{vet}^{ℓ} is the corresponding phase angle.

An analytical formulation was proposed in Ref. [8] to predict modulation sidebands of simple, single-stage planetary gear sets due to gear ME as well as rotation of the planetary carrier. In this present study, a similar analytical formulation is developed for two objectives. The first one is to demonstrate the modulation mechanism of the FET on dynamic gear mesh forces and system responses, and the second one is to investigate the combined influence of the FET and ME on modulation sidebands. The detailed formulas are given as Eqs. (9a)- (12c). For simplicity, only the fundamental harmonic of the static transmission error and time-varying gear mesh stiffness is considered. However, the following formulation could easily be expanded to include the higher harmonics as well. The parameters e_{jp}^{1}, k_{jp}^{1}, ϕ_{jp}^{1}, $(j=s,r)$ are abbreviated as e_{jp}, k_{jp}, ϕ_{jp} throughout the rest of this paper.

$$e_{spn}(t)=A_{spn}(t)e_{sp}\sin\left[B_{spn}(t)2\pi f_m t+Z_s\psi_n+\phi_{sp}\right]\tag{9a}$$

$$\begin{aligned}A_{spn}(t)=1&+\underbrace{\beta_s\sin\left(2\pi f_m t/Z_s+\phi_{\beta sn}\right)}_{\text{manufacturing errors}}\\&+\underbrace{\beta_{pn}\sin\left(2\pi f_m t/Z_p+\phi_{\beta pn}\right)}_{\text{manufacturing errors}}\\&\underbrace{\sum_{\ell=1}^{L}v_{spn}^{\ell}\sin\left(2\pi f_{vet}^{\ell}t+\phi_{vspn}^{\ell}\right)}_{\text{varying external torques}}\end{aligned}\tag{9b}$$

$$B_{spn}(t)=1+\underbrace{\hat{\beta}_s\sin\left(2\pi f_m t/Z_s+\hat{\phi}_{\hat{\beta}sn}\right)}_{\text{manufacturing errors}}+\underbrace{\hat{\beta}_{pn}\sin\left(2\pi f_m t/Z_p+\hat{\phi}_{\hat{\beta}pn}\right)}_{\text{manufacturing errors}}+\underbrace{\sum_{\ell=1}^{L}\hat{\nu}_{spn}^{\ell}\sin\left(2\pi f_{vet}^{\ell}t+\phi_{\hat{\nu}spn}^{\ell}\right)}_{\text{varying external torques}} \quad (9c)$$

In Eqs. (9a)-(9c), dimensionless coefficients ν_{spn}^{ℓ}, $\hat{\nu}_{spn}^{\ell}$ respectively represent amplitude and frequency modulations of the fundamental harmonic of $e_{spn}(t)$ due to a certain harmonic form FET with frequency of f_{vet}^{ℓ}. And parameters $\phi_{\nu spn}^{\ell}$, $\phi_{\hat{\nu}spn}^{\ell}$ denote the corresponding phase angles. As for modulation parameters associated to ME, they are not described in this paper any more since one can get them in Ref. [8], and those parameters due to ME in the following Eqs. (10a)-(12c) are not given yet.

$$e_{rpn}(t)=A_{rpn}(t)e_{rp}\times\sin\left[B_{rpn}(t)2\pi f_m t+Z_r\psi_n+\phi_{rp}+\gamma_{sr}\right] \quad (10a)$$

$$A_{rpn}(t)=1+\underbrace{\beta_r\sin\left(2\pi f_m t/Z_r+\phi_{\beta rn}\right)}_{\text{manufacturing errors}}+\underbrace{\vartheta_{pn}\sin\left(2\pi f_m t/Z_p+\phi_{\vartheta pn}+\pi\right)}_{\text{manufacturing errors}}+\underbrace{\sum_{\ell=1}^{L}\nu_{rpn}^{\ell}\sin\left(2\pi f_{vet}^{\ell}t+\phi_{\nu rpn}^{\ell}+\pi\right)}_{\text{varying external torques}} \quad (10b)$$

$$B_{rpn}(t)=1+\underbrace{\hat{\beta}_r\sin\left(2\pi f_m t/Z_r+\hat{\phi}_{\hat{\beta}rn}\right)}_{\text{manufacturing errors}}+\underbrace{\hat{\vartheta}_{pn}\sin\left(2\pi f_m t/Z_p+\hat{\phi}_{\hat{\vartheta}pn}+\pi\right)}_{\text{manufacturing errors}}+\underbrace{\sum_{\ell=1}^{L}\hat{\nu}_{rpn}^{\ell}\sin\left(2\pi f_{vet}^{\ell}t+\phi_{\hat{\nu}rpn}^{\ell}+\pi\right)}_{\text{varying external torques}} \quad (10c)$$

$$k_{spn}(t)=\bar{k}_{sp}+C_{spn}(t)k_{sp}\times\sin\left[D_{spn}(t)2\pi f_m t+Z_s\psi_n+\Gamma+\phi_{sp}\right] \quad (11a)$$

$$C_{spn}(t)=1+\underbrace{\kappa_s\sin\left(2\pi f_m t/Z_s+\phi_{\kappa sn}\right)}_{\text{manufacturing errors}}+\underbrace{\kappa_{pn}\sin\left(2\pi f_m t/Z_p+\phi_{\kappa pn}\right)}_{\text{manufacturing errors}}+\underbrace{\sum_{\ell=1}^{L}\varsigma_{spn}^{\ell}\sin\left(2\pi f_{vet}^{\ell}t+\phi_{\varsigma spn}^{\ell}\right)}_{\text{varying external torques}} \quad (11b)$$

$$D_{spn}(t)=1+\underbrace{\hat{\kappa}_s\sin\left(2\pi f_m t/Z_s+\hat{\phi}_{\hat{\kappa}sn}\right)}_{\text{manufacturing errors}}+\underbrace{\hat{\kappa}_{pn}\sin\left(2\pi f_m t/Z_p+\hat{\phi}_{\hat{\kappa}pn}\right)}_{\text{manufacturing errors}}+\underbrace{\sum_{\ell=1}^{L}\hat{\varsigma}_{spn}^{\ell}\sin\left(2\pi f_{vet}^{\ell}t+\phi_{\hat{\varsigma}spn}^{\ell}\right)}_{\text{varying external torques}} \quad (11c)$$

$$k_{rpn}(t)=\bar{k}_{rp}+C_{rpn}(t)k_{rp}\times\sin\left[D_{rpn}(t)2\pi f_m t+Z_r\psi_n+\Gamma+\gamma_{sr}+\phi_{rp}\right] \quad (12a)$$

$$C_{rpn}(t)=1+\underbrace{\kappa_r\sin\left(2\pi f_m t/Z_r+\phi_{\kappa rn}\right)}_{\text{manufacturing errors}}+\underbrace{\tau_{pn}\sin\left(2\pi f_m t/Z_p+\phi_{\tau pn}+\pi\right)}_{\text{manufacturing errors}}+\underbrace{\sum_{\ell=1}^{L}\varsigma_{rpn}^{\ell}\sin\left(2\pi f_{vet}^{\ell}t+\phi_{\varsigma rpn}^{\ell}+\pi\right)}_{\text{varying external torques}} \quad (12b)$$

$$D_{rpn}(t)=1+\underbrace{\hat{\kappa}_r\sin\left(2\pi f_m t/Z_r+\hat{\phi}_{\kappa rn}\right)}_{\text{manufacturing errors}}+\underbrace{\hat{\tau}_{pn}\sin\left(2\pi f_m t/Z_p+\hat{\phi}_{\tau pn}+\pi\right)}_{\text{manufacturing errors}}+\underbrace{\sum_{\ell=1}^{L}\hat{\varsigma}_{rpn}^{\ell}\sin\left(2\pi f_{vet}^{\ell}t+\phi_{\hat{\varsigma}rpn}^{\ell}+\pi\right)}_{\text{varying external torques}} \quad (12c)$$

where dimensionless coefficients ν_{rpn}^{ℓ}, $\hat{\nu}_{rpn}^{\ell}$, ς_{spn}^{ℓ}, $\hat{\varsigma}_{spn}^{\ell}$, ς_{rpn}^{ℓ}, $\hat{\varsigma}_{rpn}^{\ell}$ and parameters $\phi_{\nu rpn}^{\ell}$, $\phi_{\hat{\nu}rpn}^{\ell}$, $\phi_{\varsigma spn}^{\ell}$, $\phi_{\hat{\varsigma}spn}^{\ell}$, $\phi_{\varsigma rpn}^{\ell}$, $\phi_{\hat{\varsigma}rpn}^{\ell}$ can be defined similarly.

NUMERICAL ANALYSIS OF MODULATION SIDEBANDS

In order to provide a more clear demonstration of the combined influence of the FET and ME on modulation sidebands, any additional modulations associated with carrier rotations are not included in this study. A rich sideband activity in vibration spectra at a fixed position is found due to carrier rotations in Ref. [4]. Such a phenomenon could make it a less insight into the combined influence of the FET and ME on modulation sidebands.

In this section, numerical analyses are conducted with the two-stage planetary gear set illustrated in Fig.1 with and without the FET for two main objectives. The first one is to demonstrate the modulation mechanism of the FET on dynamic gear mesh forces and system responses, and the second one is to investigate the combined influence of the FET and ME on modulation sidebands. Such numerical analyses include dynamic gear mesh forces and system dynamic responses at a fixed position. In this study, dynamic responses are computed by apply-

ing the Newmark time integration method at a speed of 1750 r/min ($\Omega_s^1 = 183.26$ rad/s) representing off-resonance condition.

The basic relevant parameters of this two-stage planetary gear set are listed in Tables 1a and 1b. One can use the potential energy principle [20] to determine the mean and the fundamental harmonic values of gear mesh stiffness. As for the static transmission errors, they can be computed according to gear precision.

The following numerical analysis is conducted under one of the simplest varying external torque conditions of $\bar{T}_{vet} = 150$ Nm, $\tau_{vet}^1 = 0.3$, $f_{vet}^1 = 31$ Hz, $\phi_{vet}^1 = 0$. However, the following process can be conveniently expanded to include any more complicated the FET conditions.

Table 1a: Basic parameters of the two-stage planetary gear set

Stage	component	Tooth number	Mass (kg)	Base radius (m)	I (kg m^2)
First-stage	carrier	--	8.346	0.064	0.0332
	ring	115	9.423	0.095	0.1525
	sun	29	0.790	0.024	0.0002
	planet	43	0.620	0.035	0.0007
Second-stage	carrier	--	30.000	0.086	0.1554
	ring	85	25.000	0.120	0.6780
	sun	29	3.765	0.041	0.0026
	planet	28	1.360	0.039	0.0017

Table 1b: Basic parameters of the two-stage planetary gear set

Parameter	First-stage	Second-stage
Module (mm)	1.75	3
Pressure angle (°)	20	20
Mean mesh stiffness (N/m)	$\bar{k}_{sp} = 1.8\times10^9$, $\bar{k}_{rp} = 2.0\times10^9$	$\bar{k}_{sp} = 3.2\times10^9$, $\bar{k}_{rp} = 3.4\times10^9$
Fundamental harmonic mesh stiffness (N/m)	$k_{sp} = 5.1\times10^8$, $k_{rp} = 2.4\times10^8$	$k_{sp} = 8.7\times10^8$, $k_{rp} = 5.7\times10^8$
Transmission error (μm)	$e_{sp} = 10$, $e_{rp} = 10$	$e_{sp} = 10$, $e_{rp} = 10$
Bearing stiffness (N/m)	$k_r = k_c = k_p = 10^8$	
Torsional Stiffness (N m/rad)	$k_{r\theta} = 10^9$, $k_{s\theta} = k_{c\theta} = 0$	

Table 2: AM parameters due to manufacturing errors and the fluctuated external torque

Manufacturing errors				The fluctuated external torque			
Static gear transmission error		Time-varying gear mesh stiffness		Static gear transmission error		Time-varying gear mesh stiffness	
β_s	0.40, 0.50	κ_s	0.40, 0.50	ν_{spn}^1	0.36, 0.46	ς_{spn}^1	0.36, 0.46
$\phi_{\beta sn}$	$2\pi/3, 0, 4\pi/3$	$\phi_{\kappa sn}$	$2\pi/3, 0, 4\pi/3$	$\phi_{\nu spn}^1$	$2\pi/3, 0, 4\pi/3$	$\phi_{\varsigma spn}^1$.	$2\pi/3, 0, 4\pi/3$
β_r	0.35, 0.40	κ_r	0.35, 0.40	ν_{rpn}^1	0.32, 0.40	ς_{rpn}^1	0.32, 0.40
$\phi_{\beta rn}$	$2\pi/3, 0, 4\pi/3$	$\phi_{\kappa rn}$	$2\pi/3, 0, 4\pi/3$	$\phi_{\nu rpn}^1$	$2\pi/3, 0, 4\pi/3$	$\phi_{\varsigma rpn}^1$	$2\pi/3, 0, 4\pi/3$

Table 3: FM parameters due to manufacturing errors and the fluctuated external torque

Manufacturing errors				The fluctuated external torque			
Static gear transmission error		Time-varying gear mesh stiffness		Static gear transmission error		Time-varying gear mesh stiffness	
$\hat{\beta}_s$	4E-5, 8E-5	$\hat{\kappa}_s$	4E-5, 8E-5	$\hat{\nu}_{spn}^1$	3E-5, 5E-5	$\hat{\varsigma}_{spn}^1$	3E-5, 5E-5
$\phi_{\hat{\beta}sn}$	$2\pi/3, 0, 4\pi/3$	$\phi_{\hat{\kappa}sn}$	$2\pi/3, 0, 4\pi/3$	$\phi_{\hat{\nu}spn}^1$	$2\pi/3, 0, 4\pi/3$	$\phi_{\hat{\varsigma}spn}^1$.	$2\pi/3, 0, 4\pi/3$
$\hat{\beta}_r$	3E-5, 7E-5	$\hat{\kappa}_r$	3E-5, 7E-5	$\hat{\nu}_{rpn}^1$	3E-5, 5E-5	$\hat{\varsigma}_{rpn}^1$	3E-5, 5E-5
$\phi_{\hat{\beta}rn}$	$2\pi/3, 0, 4\pi/3$	$\phi_{\hat{\kappa}rn}$	$2\pi/3, 0, 4\pi/3$	$\phi_{\hat{\nu}rpn}^1$	$2\pi/3, 0, 4\pi/3$	$\phi_{\hat{\varsigma}rpn}^1$	$2\pi/3, 0, 4\pi/3$

Amplitude modulations

Here, ME of $E_s = 16$ μm and $E_r = 50$ μm are applied to the sun gear and ring gear for both stage while all $E_{pn} = 0$. The definitions of E_s, E_r, E_{pn} are given detailedly in Ref. [8]. The corresponding AM parameters in Eqs. (9a)-(12c) are listed in Table 2 while setting all the unlisted modulation parameters to 0. Two different values are listed in Table 2 of

β_s, the first one (0.40) is the dimensionless AM coefficient of first-stage, and the second one (0.50) is corresponding to second-stage. Similarly, the values of amplitude coefficients β_r, κ_s, κ_r, ν_{spn}^1, ν_{rpn}^1, ς_{spn}^1, ς_{rpn}^1 are listed.

Predicted dynamic gear mesh force spectra $F_{sp1}^{\mathrm{I}}(f)$, $F_{rp1}^{\mathrm{I}}(f)$ of first-stage at s/pi and r/pi meshes and $F_{sp1}^{\mathrm{II}}(f)$, $F_{rp1}^{\mathrm{II}}(f)$ of second-stage at s/pi and r/pi meshes are shown in Fig. 3. In these figures, the fundamental mesh frequencies of first-stage and second-stage are 675.2 Hz and 127.0 Hz, respectively.

As illustrated in Figs. 3(a) and 3(b), sidebands at $f = f_m^{\mathrm{I}} \pm f_m^{\mathrm{I}}/Z_s$ (675.2±23.2 Hz) and $f = f_m^{\mathrm{I}} \pm f_m^{\mathrm{I}}/Z_r$ (675.2±5.8 Hz) are evident respectively. These sidebands are caused by AM effects due to ME. The above sideband activities are highly consistent with those in Ref. [8]. Additional sidebands appear at $f = f_m^{\mathrm{I}} \pm f_{vet}^1$ (675.2±23.2 Hz) associated with AM effects due to the FET. It is also noted here that no intermodulation is found between the FET and ME when only AM effects are present. Besides, the resultant spectra indicates that the amplitude (or energy) at fundamental mesh frequency remains constant with only AM effects. Similar sideband phenomena can be found in force spectra of second-stage as illustrated in Figs. 3(c) and 3(d).

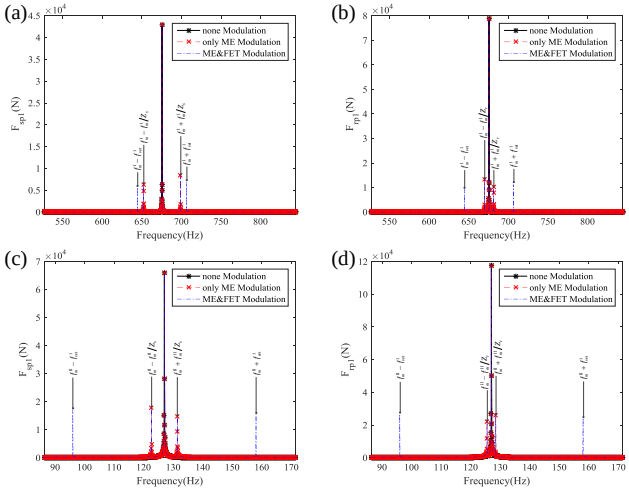

Fig. 3. Predicted dynamic gear mesh force spectra with only AM effects: (a) $F_{sp1}^{\mathrm{I}}(f)$, (b) $F_{rp1}^{\mathrm{I}}(f)$, (c) $F_{sp1}^{\mathrm{II}}(f)$, (d) $F_{rp1}^{\mathrm{II}}(f)$.

The corresponding acceleration spectra are shown in Fig. 4. Only radial acceleration spectra at a fixed position on the second-stage ring gear are given here to demonstrate the characteristics of sideband activity. Similar to dynamic gear mesh force spectra, distinct sidebands appear around the first-stage as well as the second-stage fundamental gear mesh frequency in acceleration spectra. As illustrated in Fig. 4(a), sidebands at $f = f_m^{\mathrm{I}} + f_m^{\mathrm{I}}/Z_s$ and $f = f_m^{\mathrm{I}} - f_m^{\mathrm{I}}/Z_r$ are evident when only AM effects due to ME are considered. Another additional sideband appears at $f = f_m^{\mathrm{I}} + f_{vet}^1$ due to AM effects of the FET. Sidebands around the second-stage fundamental gear mesh frequency are very similar to those around the first-stage fundamental gear mesh frequency.

Figs. 4(a) and 4(b) also clearly indicate that simpler and less symmetrical sidebands are evident compared with those in dynamic gear mesh force spectra. One potential cause for this phenomenon is the cancellation or neutralization effect of gear mesh excitations due to planet mesh phasing. It is also observed from the spectra as illustrated in Fig. 4(a) that significant responses and sidebands appear in the vicinity of the first-stage fundamental gear mesh frequency. Such a phenomenon indicates that energy of first-stage flows into second-stage, in other words, there is a significant interaction between these two adjacent stages.

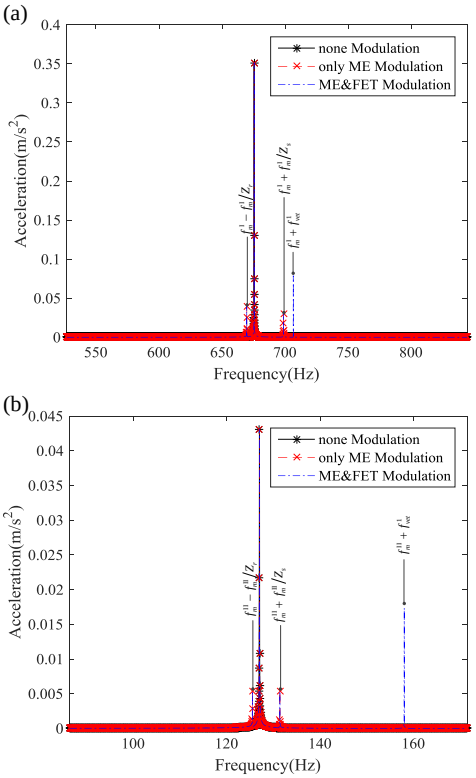

Fig. 4. Predicted radial acceleration spectra when only AM are present at a fixed position on the second-stage ring gear: (a) spectrum in the vicinity of the first-stage fundamental gear mesh frequency, (b) spectrum in the vicinity of the second-stage fundamental gear mesh frequency.

Frequency modulations

Differing from the previous case, considering only FM effects in Eqs. (9a)-(12c), the same ME, namely $E_s = 16$ μm and $E_r = 50$ μm, are used in this case. The corresponding FM parameters for this case are listed detailedly in Table 3.

The resultant dynamic gear mesh force spectra are illustrated in Figs. 5(a)-5(d). Richer and more complex sideband structures are evident compared with those in the case of AM in

Fig. 3, especially in $F_{sp1}^{\mathrm{I}}(f)$ and $F_{rp1}^{\mathrm{I}}(f)$ spectra. Taking the $F_{sp1}^{\mathrm{I}}(f)$ spectrum as an example, significant and almost symmetric sidebands appear at $f = f_m^{\mathrm{I}} \pm \lambda\, f_m^{\mathrm{I}}/Z_s$ (λ: integer) as a direct result of FM effects caused by ME. Here, besides the sidebands $f = f_m^{\mathrm{I}} \pm \lambda\, f_m^{\mathrm{I}}/Z_s$, some additional sidebands appear at $f = f_m^{\mathrm{I}} \pm \lambda\, f_m^{\mathrm{I}}/Z_s \pm \lambda_{vet}\, f_{vet}^{1}$. Such additional sidebands indicate that there is an obvious intermodulation between FM effects due to the FET and FM effects due to ME. Fig. 5(a) also clearly indicates that some energy of the first-stage fundamental gear mesh frequency is distributed to its surrounding sidebands resulting in a decrease amplitude of the gear mesh force at the first-stage fundamental gear mesh frequency. Moreover, qualitatively similar sideband activities appear in $F_{rpn}^{\mathrm{I}}(t)$, $F_{spn}^{\mathrm{II}}(t)$, $F_{rpn}^{\mathrm{II}}(t)$ spectra.

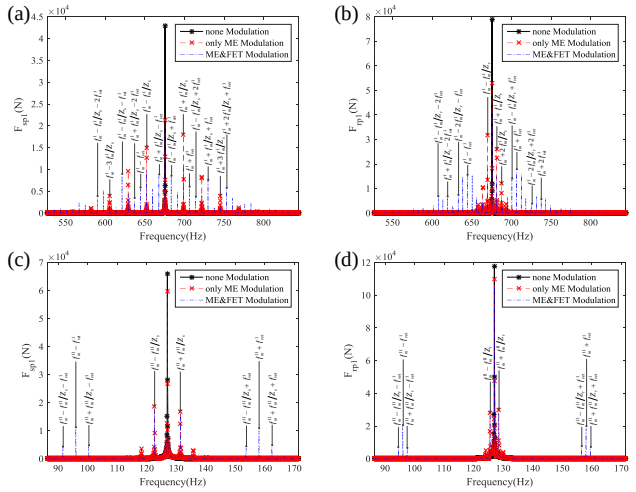

Fig. 5. Predicted dynamic gear mesh force spectra with only FM effects: (a) $F_{sp1}^{\mathrm{I}}(f)$, (b) $F_{rp1}^{\mathrm{I}}(f)$, (c) $F_{sp1}^{\mathrm{II}}(f)$, (d) $F_{rp1}^{\mathrm{II}}(f)$.

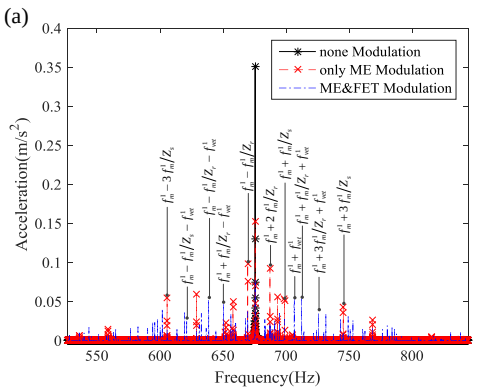

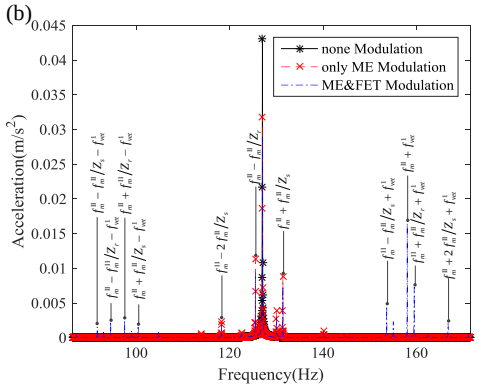

Fig. 6. Predicted radial acceleration spectra when only FM are present at a fixed position on the second-stage ring gear: (a) spectrum in the vicinity of the first-stage fundamental gear mesh frequency, (b) spectrum in the vicinity of the second-stage fundamental gear mesh frequency.

The corresponding acceleration spectra are shown in Figs. 6(a) and 6(b). Similar to gear mesh forces shown in Figs. 5(a) and 5(b), additional sidebands appear at $f = f_m^{\mathrm{I}} \pm \lambda\, f_m^{\mathrm{I}}/Z_s \pm \lambda_{vet}\, f_{vet}^{1}$ in addition to the ones at $f = f_m^{\mathrm{I}} \pm \lambda\, f_m^{\mathrm{I}}/Z_s$ as illustrated in Fig. 6(a). This phenomenon indicates again that there is an obvious intermodulation between FM effects due to the FET and FM effects due to ME. However, the symmetrical characteristic of sidebands in acceleration spectra is not as well as that in gear mesh force spectra. The resultant spectra also indicate that a significant interaction exists between these two adjacent stages.

CONCLUSIONS

Certain operating conditions such as fluctuation of the input torque to planetary gear sets were stated to cause additional sidebands in recent studies [10,11]. In order to investigate different modulation mechanisms with and without the fluctuated external torque as well as the combined influence of the fluctuated external torque and manufacturing errors on modulation sidebands, a simplified analytical model was proposed in this study. In this analytical model, gear mesh interface excitations in mesh-frequency zone are defined in Fourier series forms, and a time-varying coordinate transformation between the carrier of first-stage and the sun of second-stage to describe the coupling of the two adjacent stages.

The predicted dynamic gear mesh force spectra and radial acceleration spectra at a fixed position on ring gear were both shown to exist well-defined modulation sidebands. Comparing with sidebands caused by manufacturing errors only, more complex sidebands appeared when taking both fluctuated external torque and manufacturing errors into account. An obvious intermodulation was found around the fundamental gear mesh frequency between the fluctuated external torque and manufacturing errors in the form of frequency

modulations, however, no intermodulation in the form of amplitude modulations. The symmetrical characteristic of sidebands in acceleration spectra was not as well as that in gear mesh force spectra. Additionally, the results indicated that some of the sidebands are cancelled out in radial acceleration spectra mainly due to the effect of planet mesh phasing, especially when only amplitude modulations are present.

ACKNOWLEDGMENTS

The research work is supported by the Heilongjiang Province Funds for Distinguished Young Scientists (Grant No. JC 201405) and China Postdoctoral Science Foundation (Grant No. 2015M581433).

REFERENCES

[1] Blankenship, G. W., and Singh, R., 1995, "Analytical solution for modulation sidebands associated with a class of mechanical oscillators," J. Sound Vib., 179(1), pp. 13-36.

[2] Bellomonte, L., Guastella, I., and Sperandeo-Mineo, R. M., 2005, "Mechanical models of amplitude and frequency modulation," Eur. J. Phy., 26(3), pp. 409.

[3] McFadden, P. D., and Smith, J. D., 1985, "An explanation for the asymmetry of the modulation sidebands about the tooth meshing frequency in epicyclic gear vibration," Proc. Inst. Mech. Eng., Part C, 199(1), pp. 65-70.

[4] Inalpolat, M., and Kahraman, A., 2009, "A theoretical and experimental investigation of modulation sidebands of planetary gear sets," J. Sound Vib., 323(3-5), pp. 677-696.

[5] McFadden, P. D., 1991, "A technique for calculating the time domain averages of the vibration of the individual planet gears and the sun gear in an epicyclic gearbox," J. Sound Vib., 144(1), pp. 163-172.

[6] McNames, J., 2002, "Fourier series analysis of epicyclic gearbox vibration," ASME J. Vib. Acoust., 124(1), pp. 150-153.

[7] Mark, W. D., and Hines, J. A., 2009, "Stationary transducer response to planetary-gear vibration excitation with non-uniform planet loading," Mech. Syst. Signal Process., 23(4), pp. 1366-1381.

[8] Inalpolat, M., and Kahraman, A., 2010, "A dynamic model to predict modulation sidebands of a planetary gear set having manufacturing errors," J. Sound Vib., 329(4), pp. 371-393.

[9] Gu, X., and Velex, P., 2013, "On the dynamic simulation of eccentricity errors in planetary gears," Mech. Mach. Theory, 61, pp. 14-29.

[10] Bartelmus, W., and Zimroz, R., 2009, "Vibration condition monitoring of planetary gearbox under varying external load," Mech. Syst. Signal Process., 23(1), pp. 246-257.

[11] Bartelmus, W., and Zimroz, R., 2009, "A new feature for monitoring the condition of gearboxes in non-stationary operating conditions," Mech. Syst. Signal Process., 23(5), pp. 1528-1534.

[12] Lin, J., and Parker, R. G., 1999, "Analytical characterization of the unique properties of planetary gear free vibration," ASME J. Vib. Acoust., 121(3), pp. 316-321.

[13] Wei, J., Zhang, A. and Qin, D., et al, 2017, "A coupling dynamics analysis method for a multistage planetary gear system," Mech. Mach. Theory, 110, pp. 27-49.

[14] Zhang, A., Wei and Qin, D., et al, 2018, "Coupled Dynamic Characteristics of Wind Turbine Gearbox Driven by Ring Gear Considering Gravity," ASME J. Dyna. Syst. Meas. Cont., 140(9), 091009.

[15] Kahraman, A., 1994, "Planetary gear train dynamics," ASME J. Mech. Des., 116(3), pp. 713-720.

[16] Kahraman, A., 1994, "Load sharing characteristics of planetary transmissions," Mech. Mach. Theory, 29(8), pp. 1151-1165.

[17] Cai, Y., 1995, "Simulation on the rotational vibration of helical gears in consideration of the tooth separation phenomenon (a new stiffness function of helical involute tooth pair)," ASME J. Mech. Des., 117(3), pp. 460-469.

[18] Singh, A., 2007, "Influence of planetary needle bearings on the performance of single and double pinion planetary systems," ASME J. Mech. Des., 129(1), pp. 85-94.

[19] Abousleiman, V., Velex, P., and Becquerelle, S., 2007, "Modeling of spur and helical gear planetary drives with flexible ring gears and planet carriers," ASME J. Mech. Des., 129(1), pp. 95-106.

[20] Liang, X., Zuo, M. J., and Patel, T. H., 2014, "Evaluating the time-varying mesh stiffness of a planetary gear set using the potential energy method," Proc. Inst. Mech. Eng., Part C, 228(3), pp. 535-547.